Communication

Formation of a Nickel–Methyl Species in Methyl-Coenzyme M Reductase, an Enzyme Catalyzing Methane Formation

Na Yang, Markus Reiher, Mi Wang, Jeffrey Harmer, and Evert C. Duin

J. Am. Chem. Soc., **2007**, 129 (36), 11028-11029• DOI: 10.1021/ja0734501 • Publication Date (Web): 21 August 2007

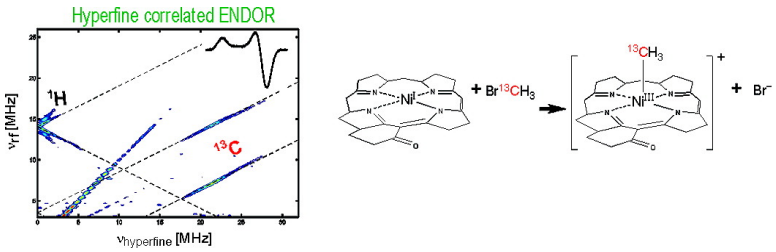

More About This Article

Additional resources and features associated with this article are available within the HTML version:

- Supporting Information
- Links to the 9 articles that cite this article, as of the time of this article download
- Access to high resolution figures
- Links to articles and content related to this article
- Copyright permission to reproduce figures and/or text from this article

View the Full Text HTML

J|A|C|S
COMMUNICATIONS

Published on Web 08/21/2007

Formation of a Nickel−Methyl Species in Methyl-Coenzyme M Reductase, an Enzyme Catalyzing Methane Formation

Na Yang,[†] Markus Reiher,[‡] Mi Wang,[†] Jeffrey Harmer,*[,§] and Evert C. Duin*[,†]

Department of Chemistry and Biochemistry, Auburn University, Alabama 36849, and Laboratory of Physical Chemistry, Department of Chemistry and Applied Biosciences, ETH-Zürich, CH-8093 Zürich, Switzerland

Received May 15, 2007; E-mail: duinedu@auburn.edu; harmer@phys.chem.ethz.ch

Methanogenesis plays an important role in the global carbon-cycle. It is the last step in the anaerobic breakdown of biopolymers in anaerobic microbial habitats. The overproduction of CH_4 due to increasing rice production and amounts of life stock has led to a steady rise in the concentration of CH_4 in the atmosphere over the last century. This is a problem since CH_4 is a potent greenhouse gas.[1] Although different compounds can be metabolized,[2] all pathways have in common the last step, the conversion of methyl-coenzyme M ($CH_3-S-CoM$) with coenzyme B ($HS-CoB$) into CH_4 and a mixed disulfide by the enzyme methyl-coenzyme M reductase (MCR):

$$CH_3-S-CoM + HS-CoB \rightarrow CH_4 + CoM-S-S-CoB$$

Central to this reaction is the nickel-containing tetrapyrrole, cofactor 430 (F_{430}). Different catalytic mechanisms have been proposed for this reaction that can in principle be divided into two basic models. In one model the key intermediate features a nickel−methyl species.[3,4] In the other model first a nickel−thiol bond is formed which subsequently results in the release of the methyl group as a methyl radical.[5] Unfortunately no direct evidence is available concerning the catalytic mechanism of this conversion. The mechanism of this enzyme has been probed with substrate analogues and inhibitors. The inhibitor coenzyme M can bind with its thiol sulfur to the nickel in the 3+, 2+, and 1+ state.[6−10] Until now a nickel−methyl species has only been detected in free Ni(I)F_{430}. In aprotic solvents, Ni(I)F_{430}M (pentamethyl ester of F_{430}) reacts with bromomethane (BrMe) to form methyl-Ni(II)F_{430}M, which subsequently can be protonolyzed to CH_4 and Ni(II)F_{430}M.[11,12] The formation of a nickel−alkyl species in MCR was first proven by reaction of MCR in the Ni(I)F_{430} state (MCR_{red1a}, "a" for absence of substrates) with 3-bromopropane sulfonate (BPS), denoted MCR_{BPS}. With the help of isotopic labeling of the C-3 carbon of this compound with ^{13}C, it was shown that upon incubation with BPS a bond was formed between the nickel (formally 3+) and the C-3 carbon.[13] Similar results were obtained with bromo-alkyl sulfonate compounds that contain longer carbon chains.[14] Here we show that a nickel−methyl species is formed when the MCR_{red1a} state is incubated with BrMe.

Incubation of a MCR_{red1a} preparation with BrMe results in the loss of the electron paramagnetic resonance (EPR) signal of this species and the formation of a new EPR signal designated MCR_{BrMe}. Complete conversion of the MCR_{red1} signal into the MCR_{BrMe} signal was achieved by incubation of 0.8 mM MCR in 50 mM Tris/HCl pH 9.0 with an approximately 50 fold excess of BrMe (added as a saturated solution in 50 mM Tris/HCl pH 9.0). The signal decays to an EPR silent form with a $t_{1/2}$ of 20 min. The electronic and geometric structure of MCR_{BrMe} was characterized in detail by CW and pulse electron nuclear double resonance (ENDOR) and hyperfine sublevel correlation (HYSCORE) spectroscopy.[15] Figure 1 shows CW EPR spectra recorded at W-band for the sample preparation MCR_{red1a}, MCR_{BrMe}, and simulation, and simulations using known g values for MCR_{BPS}[13] and MCR_{ox1}.[16] MCRox1 is the only other form with the nickel in the 3+ oxidation state. The sixth ligand however, is a thiolate sulfur from coenzyme M. Table 1 shows that upon addition of either BPS or BrMe there is a significant change in the g values in comparison to MCR_{red1a}. An X-band Davies ENDOR spectrum recorded at g_3 is shown in Figure 2A, along with the simulations for ^1H and ^{14}N signals, and a ^{13}C signal with the two carbon peaks being given by $\nu_{rf} \approx |A_3/2 \pm \nu_{13C}|$, where $A_3 = 44$ MHz and $\nu_{13C} = 3.3$ MHz (see Figure S1 and S3 for additional spectra). A HYEND (hyperfine correlated ENDOR) experiment which correlates ENDOR frequencies ν_{rf} directly against their hyperfine couplings $\nu_{hyperfine}$ was recorded at $g_{1,2}$ as shown in Figure 2B.[17] In this plot the ^{13}C signals are resolved from proton signals and the nitrogen signals are suppressed below detection. This allows the ^{13}C hyperfine couplings to be read directly from the graph, $A_{1/2} = 18$ MHz. These data are supported by X-band HYSCORE measurements (Figure S2). The large ^{13}C hyperfine coupling shows unambiguously that the methyl group from BrMe is directly coordinated to the nickel ion. The nitrogen signals in Figure 2A are assigned to the four pyrrole nitrogens of F_{430} with hyperfine couplings in the range ca. 25−35 MHz which are typical values for F_{430} when the unpaired electron is in a nickel orbital with a high $d_{x^2-y^2}$ character. It is expected that the three proton hyperfine couplings of the coordinated methyl group will have large anisotropic hyperfine couplings as they are close to the spin density, which is consistent with the ENDOR (Figure S2) and X-band HYSCORE data (Figure S4) which feature proton ridges that can be simulated with hyperfine couplings that range from −6 to +13 MHz (see Table 1).

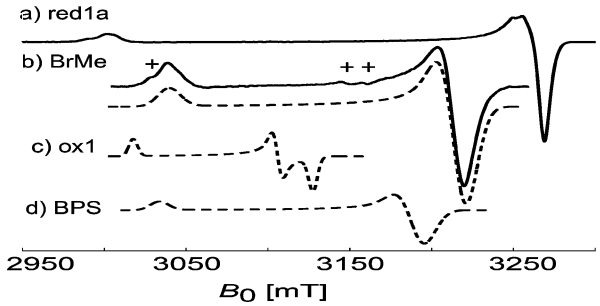

Figure 1. W-band (94.234 GHz) EPR spectra for the species MCR_{red1a} (a), MCR_{BrMe} and simulation (dotted line) (b), and simulations for using known g-values determined at W-band for MCR_{ox1} (c) and MCR_{BPS} (d). The impurity marked with + in the BrMe spectrum has g-values of 2.130, 2.139, and 2.224, amounts to ca. 2% of the signal, and is an ox3 species.

[†] Auburn University.
[‡] Laboratory of Physical Chemistry, ETH-Zürich.
[§] Department of Chemistry and Applied Biosciences, ETH-Zürich.

10.1021/ja0734501 CCC: $37.00

Table 1. *g*-Values for Several Relevant MCR Species and for MCR_{BrMe} the *g*-Values and Methyl ^{13}C and ^{1}H Hyperfine Couplings[a]

complex	g_1	g_2	g_3
MCR_{red1a}	2.061	2.070	2.250
MCR_{ox1}	2.153	2.168	2.231
MCR_{BPS}	2.108 (2.017)	2.112 (2.079)	2.219 (2.157)
MCR_{BrMe}	2.093 (2.021)	2.093 (2.062)	2.216 (2.159)
	A_1 [MHz]	A_2 [MHz]	A_3 [MHz]
$^{13}C_{Me}$[b]	-18 ± 2 (-23.7)	-18 ± 2 (-23.5)	-44 ± 2 (-42.4)
$^{1}H_{Me}$[c]	-6 to -4	1 to 3	10 to 13
	(-7.4 to -7.2)	(-0.4 to -0.1)	(7.8 to 8.0)

[a] DFT values are given in brackets; the sign of the experimental hyperfine couplings were assigned according to the calculation. [b] The tilt angle of the ^{13}C **A** matrix relative to the **g** matrix is ca. $<10°$, the simulations used 0°. [c] Experimental and DFT values show the range for the three methyl protons.

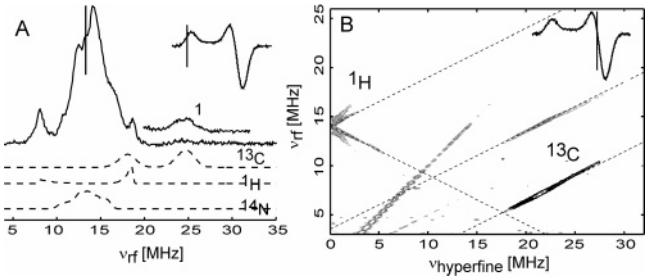

Figure 2. (A) X-band Davies ENDOR spectrum measured at the field position corresponding to g_3 (low field end, see inset). Simulations for the methyl ^{13}C and ^{1}H, and pyrrole ^{14}N nuclei are indicated by the dotted lines. The high-frequency feature of the ^{13}C signal was measured with a higher *S*/*N* (1) and is shown above the wide experimental spectrum. The horizontal line indicates the proton Larmor frequency. (B) X-band HYEND spectrum measured at the field position of $g_{1,2}$ (high field end, see inset). Protons ($A_{max} \approx 7$ MHz) and a strongly coupled ^{13}C nucleus are indicated.

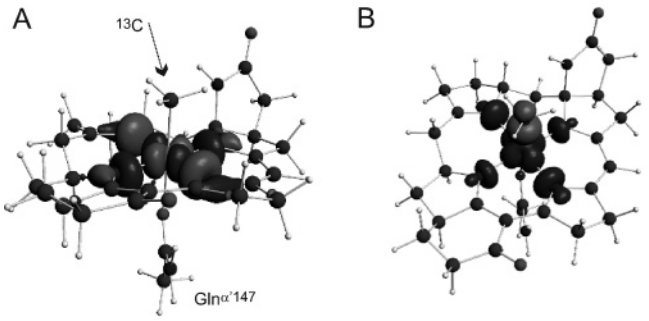

Figure 3. Plot of (A) singly occupied molecular orbital and (B) the spin density distribution (dark positive, light negative) of $H_3C-NiF^+_{430}$. Selected computed structural data: Ni−C_{Me} = 0.197, Ni−O = 0.216, Ni−N = 0.219, 0.204, 0.211, 0.202 nm. The methyl radical coordination energy is −68.2 (BP86) and −51.9 kJ/mol (B3LYP). The coordination of the oxygen of the $Gln^{\alpha'147}$ model is based on the crystal structure, but see Figure S5.

The EPR structure and parameters are fully supported by density functional theory (DFT) calculations.[18,19] The single occupied molecular orbital (SOMO) and the spin density are shown in Figure 3, and the calculated hyperfine couplings are given in brackets in Table 1. The experimental carbon hyperfine interaction is particularly well reproduced and shows that the Mulliken spin population in an s-type orbital is −1% and in the p-type orbital is −8.4% (experimental values calculated from the hyperfine interaction are 1% and 11.6%, respectively).[20] The nickel has a spin population of 81%. A comparison of the SOMO and spin density plot in Figure 3 shows that the SOMO is indeed mainly contributed to by a nickel $d_{x^2-y^2}$ orbital and that the methyl group orbitals do not contribute. The spin density plot indicates that the carbon hyperfine interaction is negative and thus results from a spin polarization mechanism. The most reasonable picture of the H_3C-Ni coordination is via an interaction of the filled nickel d_{z^2} orbital with the empty orbital from the cation CH_3^+, indicating that the bromine atom is lost as a bromide ion. This is very similar to the case where BPS is added to MCR_{red1a} to form MCR_{BPS}. DFT calculations for this species are also in excellent agreement with the experimental data, that is, $|A(^{13}C)_{exp}| = (17.6 \pm 0.5, 18.3 \pm 0.5, 45 \pm 1)$, $A(^{13}C)_{cal} = (-21.9, -21.6, -43.1)$ MHz (see Supporting Information for the SOMO, spin density, and other EPR parameters).

Experimental detection of a methyl−nickel species in the active site of MCR adds plausibility to proposed mechanisms proceeding via such intermediates with the natural substrates. Since Ni(III) species are strong oxidants, species such as $H_3C-Ni^{III}F^+_{430}$ may play a crucial role in C−H activation for "reverse methanogenesis", that is, anaerobic oxidation of methane.[21]

Acknowledgment. This work was supported by the Petroleum Research Fund (E.D.), the ETH, and the Swiss National Science Foundation (J.H.).

Supporting Information Available: Experimental methods, Figures S1−S8, and Tables S1−S5. This material is available free of charge via the Internet at http://pubs.acs.org.

References

(1) Conrad, R. *Microbiol. Rev.* **1996**, *60*, 609−640.
(2) Thauer, R. K. *Microbiol.* **1998**, *144*, 2377−2406.
(3) Grabarse, W.; Mahlert, F.; Duin, E. C.; Goubeaud, M.; Shima, S.; Thauer, R. K.; Lamzin, V.; Ermler, U. *J. Mol. Biol.* **2001**, *309*, 315−330.
(4) Horng, Y.-C.; Becker, D. F.; Ragsdale, S. W. *Biochemistry* **2001**, *40*, 12875−12885.
(5) Pelmenschikov, V.; Siegbahn, P. E. M. *J. Biol. Inorg. Chem.* **2003**, *8*, 653−662.
(6) Duin, E. C.; Signor, L.; Piskorski, R.; Mahlert, F.; Clay, M. D.; Goenrich, M.; Thauer, R. K.; Jaun, B.; Johnson, M. K. *J. Biol. Inorg. Chem.* **2004**, *9*, 563−576.
(7) Craft, J. L.; Horng, Y. C.; Ragsdale, S. W.; Brunold, T. C. *J. Biol. Inorg. Chem.* **2004**, *9*, 77−89.
(8) Ermler, U.; Grabarse, W.; Shima, S.; Goubeaud, M.; Thauer, R. K. *Science* **1997**, *278*, 1457−1462.
(9) Telser, J.; Davydov, R.; Horng, Y.-C.; Ragsdale, S. W.; Hoffman, B. M. *J. Am. Chem. Soc.* **2001**, *123*, 5853−5860.
(10) Finazzo, C.; Harmer, J.; Bauer, C.; Jaun, B.; Duin, E. C.; Mahlert, F.; Goenrich, M.; Thauer, R. K.; Van Doorslaer, S.; Schweiger, A. *J. Am. Chem. Soc.* **2003**, *125*, 4988−4989.
(11) Jaun, B.; Pfaltz, A. *J. Chem. Soc., Chem. Commun.* **1988**, 293−294.
(12) Lin, S.-K.; Jaun, B. *Helv. Chim. Acta* **1991**, *74*, 1725−1738.
(13) Hinderberger, D.; Piskorski, R.; Goenrich, M.; Thauer, R. K.; Schweiger, A.; Harmer, J.; Jaun, B. *Angew. Chem., Int. Ed. Engl.* **2006**, *45*, 3602−3607.
(14) Kunz, R. C.; Horng, Y. C.; Ragsdale, S. W. *J. Biol. Chem.* **2006**, *281*, 34663−34676.
(15) Schweiger, A.; Jeschke, G. *Principles of Pulse Electron Paramagentic Resonance*; Oxford Press: Oxford, 2001.
(16) Harmer, J.; Finazzo, C.; Piskorski, R.; Bauer, C.; Jaun, B.; Duin, E. C.; Goenrich, M.; Thauer, R. K.; Van Doorslaer, S.; Schweiger, A. *J. Am. Chem. Soc.* **2005**, *127*, 17744−17755.
(17) Jeschke, G.; Schweiger, A. *Chem. Phys. Lett.* **1995**, *246*, 431.
(18) Geometry optimizations and bond energies were calculated with TurboMol and single-point calculations with the Amsterdam density functional package. Details are given in the Supporting Information.
(19) Wondimagegn, T.; Ghosh, A. *J. Am. Chem. Soc.* **2001**, *123*, 1543−1544.
(20) The experimental spin population in a p-orbital is calculated as *T*/74 MHz, and in an s-orbital as a_{iso}/2901 MHz, where for an axial hyperfine interaction with principal values ($A_\perp$, $A_\perp$, $A_\parallel$) the dipolar part $T = A_{\perp\nu} - a_{iso}$ and the isotropic part $a_{iso} = (A_\parallel + 2A_\perp)/3$. The constants 74 and 2901 MHz were determined from our DFT data and are very similar to values calculated for the isolated atoms, see for example: (a) Morton, J. R.; Preston, K. F.; *J. Magn. Reson.* **1978**, 30, 577−582. (b) Koh, A. K.; Miller, D. J.; *At. Data Nucl. Data Tables* **1985**, *33*, 235−253.
(21) Shima, S.; Thauer, R. K. *Curr. Opin. Microbiol.* **2005**, *8*, 643−648.

JA0734501